or

$$\int_0^{\tau} \partial_t \langle \boldsymbol{J}(\boldsymbol{R}, \theta, t)\rangle \, \mathrm{d}\theta + \langle \boldsymbol{J}(\boldsymbol{R}, t, t)\rangle = -\lambda \nabla T - \sigma \hat{n}(\nabla \cdot \boldsymbol{u}) \quad (14)$$

where $E^{\text{int}} = -|E^{\text{int}}|$ for bound states.[7] With the use of Ergodic theory,[1] Eq. (14) will immediately lead to

$$\tau \frac{\partial \langle \boldsymbol{J}(\boldsymbol{R}, t)\rangle}{\partial t} + \langle \boldsymbol{J}(\boldsymbol{R}, t, t)\rangle = -\lambda \nabla T - \sigma \hat{n}(\nabla \cdot \boldsymbol{u}) \quad (15)$$

which is the non-Fourier heat-flux law for diatomic gases, given that the gas is incompressible. If Eq. (1) is used in the equation for β^*_{int} and the assumption that $W(r_m)$ and $\langle E^{\text{tr}}\rangle$ are uncorrelated is applied, one gets $\beta^*_{\text{int}} = 3\{1 - [\mu(\delta v)^2/3k_BT] + 2W(r_m)/3k_BT\}$. Furthermore, because the pair correlation has a single maximum for low densities that occurs at r_m for the Lennard–Jones potential,[5] which represents gases, one may substitute the value of the Lennard–Jones potential[2] at r_m for $W(r_m)$. Then, assuming it to be at the critical temperature, one gets the equation[2] $W(r_m) = -0.77k_BT_c$, where the minus sign is caused by the fact that the bound state is considered. Assuming the validity of the equations $u_M^2 = (8k_BT_c/\pi M)$, $\langle V^2\rangle = (3k_BT_c/M)$, $u_\mu^2 = (8k_BT_c/\pi\mu)$, and $\langle v^2\rangle = (3k_BT_c/\mu)$ at the critical temperature, one gets $\beta^*_{\text{int}} = 1.007$. The value for β^*_{int} obtained by Eucken is unity.[6] On the other hand, $\beta^*_{\text{tr}} = 3 - 3 + (8/\pi) = 2.547$, and $\beta^*_{\text{dia}} = 2.547 - 0.667(1.007) = 1.875$ at $T = T_c$, where the value of γ is taken to be $\gamma = 1.4$ for diatomic gases. The value for β^*_{dia} obtained by Eucken is 1.94. The closeness of these numbers can be taken as an indication of the correct approach. For a van der Waals gas the translational energy will have an extra term that is independent of temperature, which will give the same Eucken number. This could be caused by the fact that the statistical formalism of a diatomic gas takes into account the effects of the van der Waals gas model. For example, the fixed distance between the two point particles generates over time a spherically symmetric shape when all of the rotations are considered. This spherically symmetric shape resembles the volume of a monoatomic van der Waals gas molecule. In addition, the van der Waals gas considers pair potentials, which is the same type of potential that is considered when one deals with the statistical description of diatomic gases.

Appendix: Internal Energy in Exponential Form

In general, the average internal energy is given by

$$\langle E^{\text{int}}\rangle = \langle E^{\text{kin}}\rangle + \langle E^{\text{pot}}\rangle \quad (A1)$$

Because setting $W(r) = W(r_m)$ indicates negligible kinetic energy caused by radial motion, the value of $\langle E^{\text{kin}}\rangle$ equals k_BT at equilibrium and local equilibrium as well. The value of $\langle E^{\text{pot}}\rangle$ is expected to be a multiple of k_BT, and one can write

$$\langle E^{\text{int}}\rangle = \langle E^{\text{kin}}\rangle + q\langle E^{\text{kin}}\rangle \quad (A2)$$

where $\langle |E^{\text{pot}}|\rangle = q\langle E^{\text{kin}}\rangle$. If one writes

$$q = \sum_{\ell=1}^{\infty} [\beta W(r_m)]^{\ell}/\ell!$$

and chooses the Lennard–Jones potential $W(r_m) = -0.77k_BT_c$, one gets $q = 0.537$. Therefore, assuming small oscillations about r_m, one gets $\langle E^{\text{kin}}\rangle = k_BT_c$, which will lead to $\langle |E^{\text{pot}}|\rangle = 0.537k_BT_c$, which is about the average energy contribution from a harmonic oscillator. This is consistent with our assumption to set $W(r) = W(r_m)$, which states that the two particles may be in the neighborhood of a fixed equilibrium distance. Therefore, for temperatures in the neighborhood of T_c, Eq. (A2) can be written as

$$\langle E^{\text{int}}\rangle = \langle E^{\text{kin}}\rangle \exp[\beta W(r_m)] \equiv \langle E^{\text{int}}(v)\rangle \exp[\beta W(r_m)] \quad (A3)$$

From Eq. (A3) one gets $E^{\text{int}}(v, r_m) = E^{\text{int}}(v)\exp[\beta W(r_m)]$. The equation

$$\int_{\Gamma} \mathrm{d}^3 r g(r_m)$$

can be integrated to give

$$\Gamma g(r_m) = 1/n \quad (A4)$$

Acknowledgments

Gratitude is acknowledged to Ronald B. Guenther and Ernest L. Roetman for their important follow-up and evaluation of this work.

References

[1] Ali, A. H., "Statistical Mechanical Derivation of Cattaneo's Heat Flux Law," *Journal of Thermophysics and Heat Transfer*, Vol. 13, No. 4, 1999, pp. 544–546.

[2] Hirschfelder, J. O., Curtiss, C. F., and Bird, R. B., *Molecular Theory of Gases and Liquids*, Wiley, New York, 1954, pp. 32, 245, 454, 498.

[3] Singwi, K. S., Tosi, M. P., Land, R. H., and Sjölander, A., "Electron Correlations at Metallic Densities," *Physical Review*, Vol. 176, 1968, pp. 589–599.

[4] Chandler, D., *Introduction to Modern Statistical Mechanics*, Oxford Univ. Press, New York, 1987, pp. 195–201.

[5] Hansen, J. P., and McDonald, I. R., *Theory of Simple Liquids*, Academic, Orlando, FL, 1986, pp. 18, 67.

[6] Tien, C. L., and Lienhard, J. H., *Statistical Thermodynamics*, Holt, Rinehart, and Winston, Philadelphia, 1971, pp. 311–313.

[7] Jeans, J. H., *The Dynamical Theory of Gases*, Dover, New York, 1954, pp. 184–186, 195.

Thermal Contact Conductance of Metal/Polymer Joints

J. J. Fuller* and E. E. Marotta†
Clemson University,
Clemson, South Carolina 29634-0921

Introduction

POLYMERS and organic materials are being employed to a greater extent in power generating systems, and with greater use follows an increased interest in the thermal transport properties of polymers. These properties include thermal conductivity, heat capacity, and the thermal contact conductance at the interface with other materials. One important consideration where limited knowledge exists is the heat flow across a metal/polymer interface. Currently, a usable and verifiable model does not exist for predicting the thermal performance of metal/polymer joints.

Marotta and Fletcher[1] measured the thermal conductivity and the thermal contact conductance of several widely available thermoplastic and thermosetting polymers. They compared the experimentally measured data with the current thermal contact models developed for metal/metal contact, such as the elastic contact model developed by Mikic[2] and the plastic contact model developed by Cooper et al. (CMY).[3] The Mikic and CMY models are accepted and proven for metal/metal contacts, but it was observed that a new thermal contact model was needed for a metal in contact with a much softer polymer layer with either finite or infinite length (half-space solution).

Problem Statement

The goal was to obtain a verifiable and usable analytical model for the prediction of thermal joint resistance between a metal and a polymer. The scope of this investigation was limited to assuming

Received 17 May 1999; presented as Paper 99-3490 at the AIAA 33rd Thermophysics Conference, Norfolk, VA, 28 June–1 July 1999; revision received 1 October 1999; accepted for publication 11 October 1999.

*Research Assistant, Department of Mechanical Engineering. Member AIAA.

†Assistant Professor, Department of Mechanical Engineering. Member AIAA.

nearly optically flat surfaces at a uniform interface pressure, a vacuum environment, and to the class of thermoplastic and elastomeric polymers. The desire was to develop an analytical model from surface contact mechanics principles that incorporates the polymer's basic properties to make the model more accurate.

The joint resistance to heat flow, which incorporates the bulk properties of the polymer, can be defined as

$$R_j = R_{\text{micro},1} + R_{\text{bulk}} + R_{\text{micro},2} \tag{1}$$

where R_{micro} is the thermal contact resistance at the interface and R_{bulk} is the thermal resistance due to the bulk properties of the polymer. By redefining the resistance using the definition of conductance, Eq. (1) can be written as

$$h_j = 1/(1/h_{\text{micro},1} + 1/h_{\text{bulk}} + 1/h_{\text{micro},2}) \tag{2}$$

An interesting fact in bare metal to metal contacts is that the real contact area is always less than the apparent contact area A, yet because thermoplastic and elastomeric polymers have comparatively lower modulus of elasticity, the calculated real contact area can actually be greater than the apparent area.

In relation to the thermal contact conductance, this increase in contact area as it approaches and then becomes greater than the apparent contact area will cause the contact resistance to become negligible. The contact mechanics behavior of the interface is why a joint conductance has been chosen to be modeled. A joint conductance model will be able to incorporate the microscopic resistance at low loads, both the microscopic and bulk resistance at intermediate loads, and then the bulk resistance at the higher loads.

The present analytical model is compared to experimental data previously gathered by Marotta and Fletcher[1] for common polymers: Delrin®, Teflon®, polycarbonate, and polyvinyl chloride (PVC). These polymers were chosen based on their commercial importance in current engineering applications and the availability of their material properties from standard chemical handbooks. The four polymers also displayed a range of Young's modulus between 5.52×10^8 and 4.14×10^9 Pa.

For the present investigation, the mode of deformation between the metal and the softer polymer is assumed to be elastic during light to moderate loading. This assumption is supported by the experimental study conducted by Parihar and Wright,[4] in which the rms roughness and the asperity slope of the steel flux meters and the silicone specimen before and after loading was measured. The measured values remained unchanged, which, they concluded, implies elastic deformation during the loading and unloading cycle.

Note the thickness of the elastic layer t. Because the polymer layer is usually in contact with a much harder underlying substrate, that is, Al 6101-T6, the substrate could affect the contact mechanics of the metal/polymer joint. Makushkin[5] studied the influence of the underlying substrate and the thickness of an elastic layer during spherical indentor penetration. He derived a mathematical expression for the critical polymer layer thickness t^* beyond which the substrate will not influence the deformation of the elastic layer:

$$t^* = 16.8\left(\frac{\sigma_t \rho}{E_p}\right)\left[\frac{(E_p/E_s)^{0.11}}{\nu_p^{0.41}\nu_s^{0.003}}\right] \tag{3}$$

By the use of the geometric properties measured by Marotta and Fletcher,[1] the critical polymer thickness for the four selected polymers were calculated and are as follows: Teflon 80.0 μm, Delrin 26.1 μm, PVC 17.2 μm, and polycarbonate 28.2 μm. The thickness of the polymers employed by Marotta and Fletcher[1] ranged from 1.65 to 12.7 mm, which is well above the calculated critical polymer thickness for the respective polymer.

The next step was to define the microscopic and bulk resistance. A possible candidate for defining the microscopic resistance was the well-established Mikic elastic model. The dimensionalized contact conductance h_c was defined by Mikic[2] as

$$h_c = \frac{k_s}{4\sqrt{\pi}}\frac{m_{ab}}{\sigma}\frac{\exp(-\lambda^2/2)}{\left[1 - \sqrt{\frac{1}{4}\operatorname{erfc}(\lambda/\sqrt{2})}\right]^{1.5}} \tag{4}$$

where λ is the dimensionless separation distance and is defined as

$$\lambda = \sqrt{2}\,\operatorname{erfc}^{-1}(4P/H_e) \tag{5}$$

The Mikic model assumes the elastic mode of deformation of the asperities, but the elastic hardness is defined for metal/metal contacts and not metal/polymer contacts. By assuming a Gaussian distribution of asperity heights, Greenwood and Williamson[6] showed that the area of contact of nominally flat surfaces is almost exactly proportional to the load. They define an elastic contact hardness that controls the area of contact by $H_{\text{elastic}} = CEm_{ab}$, where C is a constant found by plotting dimensionless mean pressure vs dimensionless load. In the present investigation, the constant was found to be approximately 0.433; therefore, a polymer elastic hardness was defined as

$$H_{ep} = E_p m_{ab}/2.3 \tag{6}$$

By inserting the new polymer elastic hardness into Eqs. (4) and (5), the predicted microscopic contact conductance was obtained. Figure 1 shows a plot of the dimensionless contact conductance as a function of dimensionless interface pressure incorporating the new polymer elastic hardness. With the use of the analytical model and polymer elastic hardness, a simple correlation was obtained for the dimensionless microscopic contact conductance:

$$\frac{h_c\sigma}{k_s m_{ab}} = 1.49\left(\frac{2.3P}{E_p m_{ab}}\right)^{0.935} \tag{7}$$

The bulk thermal conductance term was defined as

$$h_{\text{bulk}} = k_p/t_f \tag{8}$$

where t_f is the polymer's final thickness after load compression. Note that because the polymer is modeled as an elastic and compressible layer that the thickness will be a function of load. By defining the final thickness it terms of strain, the following expression was derived:

$$t_f = t_o[1 - (P/E_p)] \tag{9}$$

By substituting Eqs. (8) and (9) into Eq. (2), the joint conductance was defined as

$$h_j = 1\Big/\left\{\frac{1}{h_{\text{micro},1}} + \frac{t_o[1 - (P/E_p)]}{k_p} + \frac{1}{h_{\text{micro},2}}\right\} \tag{10}$$

Summary and Discussion

The present joint conductance model was compared with the published data of Marotta and Fletcher.[1] They reported an 11.7% uncertainty in the thermal conductivity values and an uncertainty of 16.7% in the thermal contact conductance values. The experimental data of Marotta and Fletcher[1] were gathered with the use of thermal grease applied to contact surface 2. The thermal grease allows for almost total area contact between the polymer and the metal, thus causing the $1/h_{mc,2}$ term to be negligible. By neglecting the resistance at interface 2, Eq. (10) reduces to the following expression:

$$h_{j,p} = 1\Big/\left\{\frac{1}{h_{\text{micro},1}} + \frac{t_o[1 - (P/E_p)]}{k_p}\right\} \tag{11}$$

Equation (11) was employed for comparison to the experimental data.

Figure 2 compares the joint conductance model to Marotta and Fletcher's[1] experimental data using the microscopic conductance model defined by the polymer elastic hardness. The dimensionless joint conductance was plotted vs the dimensionless load. As one

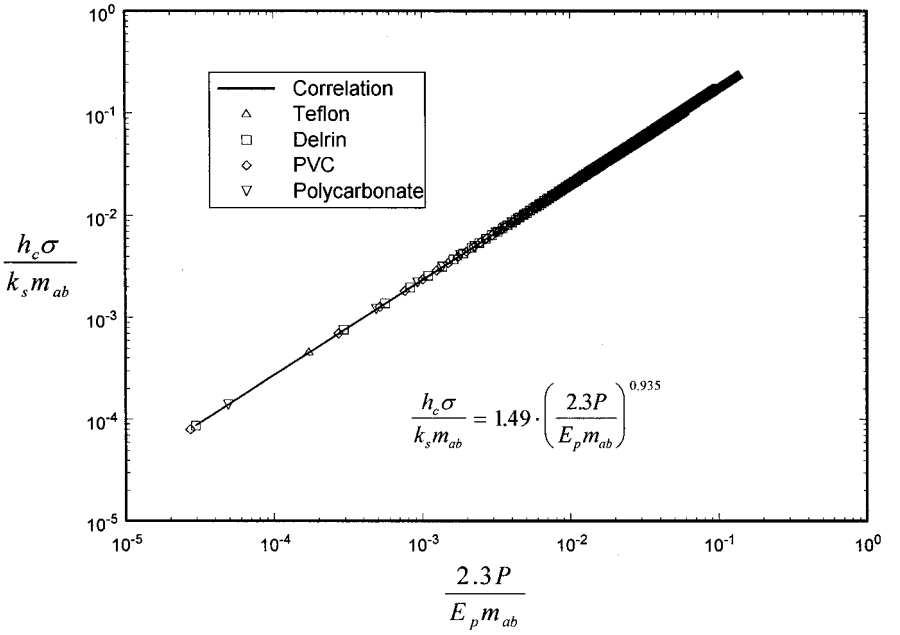

Fig. 1 Dimensionless contact conductance vs dimensionless pressure for selected polymers: correlation equation.

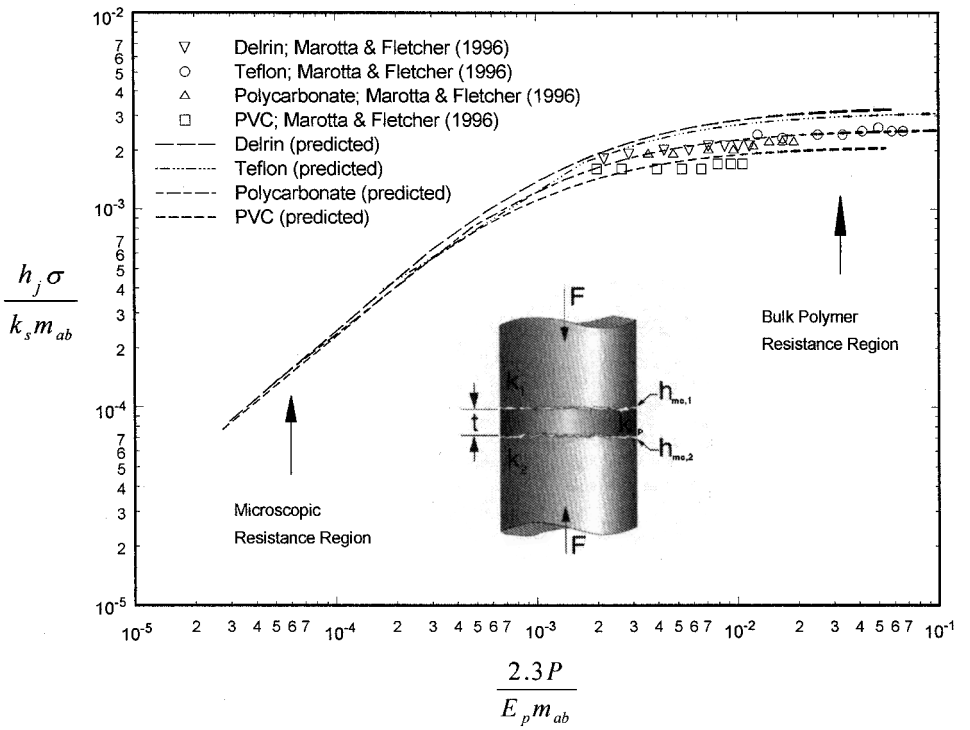

Fig. 2 Dimensionless joint conductance vs dimensionless load: alternative microscopic model with experimental data.

can observe, the data compare quite favorably with the joint conductance model. By the plotting of the data against the joint conductance model, it is indicated why the measured resistances were fairly independent of pressure. It was observed that the experimental data were taken at loads where most of the influence of the contact resistance had become negligible. Marotta and Fletcher had mainly measured the bulk resistance of the respective polymer, which is not a function of load.

Conclusion

In conclusion, a joint conductance model has been proposed for predicting the heat transfer across a metal/polymer joint. The joint conductance model includes both the resistance due to the microscopic contact heat transfer and resistance due to the bulk properties of the polymer. A new polymer elastic hardness has been defined to predict better the contact mechanics at the interface.

Because of the limited amount of published data, an experimental study is needed to completely verify the joint conductance model, especially at light loads. In real applications, Young's modulus of a polymer is a function of temperature; therefore, it is desired to include an expression for the Young's modulus as a function of temperature into the joint conductance model and also to investigate the effect of nonuniform pressure distributions.

Acknowledgments

The authors would like to especially thank M. Yovanovich for his insights and helpful discussions, as well as B. Mikic for several publications provided to us.

References

[1]Marotta, E. E., and Fletcher, L. S., "Thermal Contact Conductance of Selected Polymeric Materials," *Journal of Thermophysics and Heat Transfer*, Vol. 10, No. 2, 1996, pp. 334–342.

[2]Mikic, B. B., "Thermal Contact Conductance; Theoretical Considerations," *International Journal of Heat and Mass Transfer*, Vol. 17, 1974, pp. 205–214.

[3]Cooper, M., Mikic, B. B., and Yovanovich, M. M., "Thermal Contact Conductance," *International Journal of Heat and Mass Transfer*, Vol. 12, 1969, pp. 279–300.

[4]Parihar, S. K., and Wright, N. T., "Thermal Contact Resistance at Elastomer to Metal Interfaces," *International Communications in Heat and Mass Transfer*, Vol. 24, No. 8, 1997, pp. 1083–1092.

[5]Makushkin, A. P., "Study of Stress-Strain of Polymer Layer During Spherical Indenter Penetration," *Trenie I Iznos*, Vol. 5, No. 5, 1984, pp. 823–832.

[6]Greenwood, J. A., and Williamson, J. B. P., "Contact of Nominally Flat Surfaces," *Proceeding of the Royal Society of London, Series A: Mathematical and Physical Sciences*, Vol. A295, 1966, pp. 300–319.

Impingement Heat Transfer Measurements Under an Array of Inclined Jets

Srinath Ekkad*
Louisiana State University, Baton Rouge, Louisiana 70803
and
Yizhe Huang† and Je-Chin Han‡
Texas A&M University, College Station, Texas 77843

Introduction

JET impingement is a commonly used technique for heat transfer enhancement. Several applications such as heat treatment of metals, paper drying, electronic component cooling, and turbine component cooling have benefitted from the high heat transfer rate associated with jet impingement. Several geometrical and flow parameters are known to affect the heat transfer rate for jet impingement. Perry,[1] Chupp et al.,[2] Kercher and Tabakoff,[3] Flourschuetz et al.,[4,5] Behbahani and Goldstein,[6] and Downs and James[7] studied the effects of various parameters relating to jet impingement heat transfer. All of these studies had orthogonal jet impingement. They summarized the effects of geometry, temperature, interference and crossflow, turbulence levels, surface curvature, and nonuniformity of jet array on heat and mass transfer.

Goldstein and Franchett,[8] Steven and Webb,[9] and Ichimaya[10] studied the effects of inclined jet impingement and found that inclined jets produce less heat transfer enhancement than orthogonal jets. However, they did not investigate the effects of crossflow on inclined jet impingement. Huang et al.[11] studied the effect of crossflow direction on jet impingement heat transfer for orthogonal impinging jets. They reported the highest heat transfer coefficients for the jets where the crossflow exits in both directions. The present study investigates the same crossflow effects of Huang et al.[11] for inclined jet impingement.

The present study provides detailed surface heat transfer coefficient distributions for the target plate using a transient liquid crystal technique. This is the same methodology applied by the same group of authors as in the studies by Huang et al.[11] and Ekkad et al.[12] In the present study, the effect of crossflow direction and jet inclination angle is presented for a single jet average Reynolds number of 1.28×10^4.

Received 9 August 1999; revision received 19 November 1999; accepted for publication 24 November 1999.

*Assistant Professor, Mechanical Engineering Department. Member AIAA.

†Research Assistant, Department of Mechanical Engineering; currently Project Engineer, Motorola, Inc., Austin, TX 78712.

‡Heat Transfer Research Institute Professor, Department of Mechanical Engineering. Associate Fellow AIAA.

Test Description and Apparatus

A detailed description of the test setup and instrumentation is provided by Huang et al.[11] The test section has been modified to accept jet impingement plates with inclined angled holes. There are 48 impingement holes of 0.635-cm diam arranged in an array of 12 columns and 4 rows. The jet-to-jet spacing S/d is four hole diameters. The jet plate to target plate spacing H/d (shortest distance between jet hole plate and target plate) is three hole diameters. The flow enters the pressure plenum through a narrow channel and exits through the impingement holes and impinges on the target surface. The flow exit (crossflow) direction can be altered by changing the discharge openings after impingement. Figure 1 shows the schemes of the impinging jets at ±45 deg to the vertical on to the target plate. Cases 1–3 are for different crossflow directions for the +45-deg angled jets, and cases 4–6 are for different crossflow directions for the −45-deg angled jets. The axial location is measured from the inlet side of the pressure plenum before impingement. The plate length X is normalized with the hole diameter d from 0 to 48. The hole L/d ratio is 1.0 for the orhtogonal jets and is 1.41 for the inclined jets. The hole length is not long enough to provide a fully developed and directed jet. However, the jet appears to be inclined sufficiently to provide different surface heat transfer results than for the orthogonal jets.

To avoid redundancy, details on the experimental technique and test procedure are not repeated. Huang et al.[10] and Ekkad et al.[11] describe the test section, experimental technique, and testing procedure in detail. A transient liquid crystal technique is used to obtain the two-dimensional surface heat transfer coefficient distributions. The test surface is coated with a thin layer of thermochromic liquid crystals. A heated flow is suddenly directed into the test section. The time of color change from colorless to green at every pixel location on the target surface is measured using the image processing system. The heat transfer coefficient at every location is calculated using the one-dimensional transient conduction equation and a semi-infinite solid assumption. The average experimental uncertainty in the heat transfer coefficient measurement is around ±6.4% with a maximum of around ±10% near edges.

Results and Discussion

Figure 2 presents the detailed Nusselt number ($Nu = hd/k_{air}$) distributions on the target plate for the six cases shown in Fig. 1 at a jet average Reynolds number ($Re_j = \rho V_j d/\mu$) of 1.28×10^4. The results are presented from $X/d = 3.5$ to 44.5. The total length to jet hole diameter ratio of the target plate is 48. The measurements are presented over the entire span of the test section, $Y/d = 24$. Figure 2a shows the detailed Nusselt number distributions for the

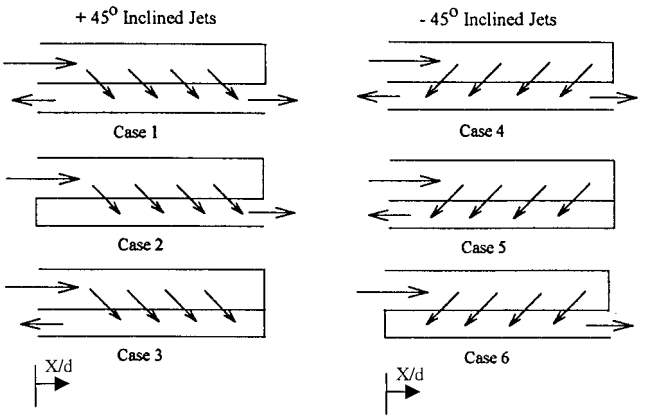

Fig. 1 Schematic of the inclined jet geometry and crossflow directions, cases 1–6.